The Journal of Chemical Physics

RESEARCH ARTICLE | DECEMBER 02 2024

Efficient method for simulating ionic fluids between polarizable metal electrodes

Igor M. Telles ; Alexandre P. dos Santos ; Yan Levin

Check for updates

J. Chem. Phys. 161, 214102 (2024)
https://doi.org/10.1063/5.0233310

View Online
Export Citation

Articles You May Be Interested In

Electrolytes in conducting nanopores: Revisiting constant charge and constant potential simulations

J. Chem. Phys. (September 2024)

Ions at electrochemical interfaces: From explicit to implicit molecular solvent descriptions

J. Chem. Phys. (July 2025)

Effects of electrostatic coupling and surface polarization on polyelectrolyte brush structure

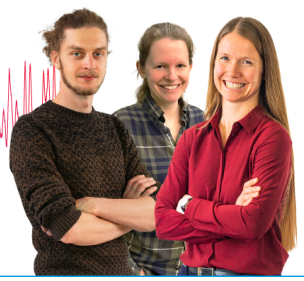
J. Chem. Phys. (April 2023)

01 December 2025 18:34:50

Webinar From Noise to Knowledge

May 13th – Register now

Zurich Instruments
Universität Konstanz



AIP Publishing

The Journal of Chemical Physics ARTICLE pubs.aip.org/aip/jcp

Efficient method for simulating ionic fluids between polarizable metal electrodes

Cite as: J. Chem. Phys. 161, 214102 (2024); doi: 10.1063/5.0233310
Submitted: 13 August 2024 • Accepted: 12 November 2024 •
Published Online: 2 December 2024

View Online Export Citation CrossMark

Igor M. Telles,[a] Alexandre P. dos Santos,[b] and Yan Levin[c]

AFFILIATIONS

Instituto de Física, Universidade Federal do Rio Grande do Sul, Caixa Postal 15051, CEP 91501-970 Porto Alegre, RS, Brazil

[a]Electronic mail: igor.morais@ufrgs.br
[b]Author to whom correspondence should be addressed: alexandre.pereira@ufrgs.br
[c]Electronic mail: levin@if.ufrgs.br

ABSTRACT

We introduce an efficient method for simulating Coulomb systems confined by conducting planar surfaces. The new approach is suitable for both coarse-grained models and all-atom simulations of ionic liquids between polarizable metal electrodes. To demonstrate its efficiency, we use the new method to study the differential capacitance of an ionic liquid. Our technique is at least two orders of magnitude faster than traditional Ewald-based methods for non-polarizable surfaces, when calculating the electrostatic energy between two ions. This advancement has significant potential to enhance understanding in fields such as materials science and electrochemistry, enabling efficient large-scale simulations of Coulomb systems confined by polarizable metal electrodes.

Published under an exclusive license by AIP Publishing. https://doi.org/10.1063/5.0233310

01 December 2025 18:34:50

I. INTRODUCTION

Simulating charged systems poses computational challenges, necessitating advanced methodologies to accurately account for forces and periodic boundary conditions. The widely adopted Ewald summation method, augmented with geometrical corrections,[1,2] is effective for studying confined systems such as electrolytes in slab[3–5] and cylindrical geometries.[6–8] However, difficulties arise when ionic fluids and the confining material have different dielectric properties. Surface polarization effects can be explored by minimizing the electrostatic energy, utilizing discontinuities in the displacement field,[9–13] or using periodic Green functions.[14] The approach based on periodic Green functions facilitates the study of electrokinetic phenomena in various geometries, particularly those with dielectric mismatches.[15,16] The investigation of systems with metallic characteristics, including polyelectrolyte brushes,[17,18] metal nanoparticles,[19–21] ionic liquids,[22–25] and supercapacitors,[26–29] holds significant importance across various fields. The existing methods, usually, encounter challenges when applied to charged systems confined by conducting surfaces.[30] Techniques such as fluctuating charges,[31–33] Gaussian function representation of surface charges,[34] Green functions,[35] and direct summations of image charges with mapping or lattice schemes[36–39] often face difficulties related to the complexity of the interaction potential and slow convergence. The problem becomes even more challenging if one considers surfaces that are not perfect conductors.[25,40] Some studies enhance computational efficiency by integrating standard electrostatic solvers into the simulation of constant potential electrodes.[41] The simulation technique that explicitly models the charge flow to and from the electrodes is used to explore the charging and discharging mechanisms of supercapacitors through molecular dynamics simulations.[42] Other approaches consider virtual particles that mimic the polarization effects by using a polarizable Lennard-Jones potential similar to the Lorentz–Drude model.[43] Moreover, tools such as MetalWalls,[44] LAMMPS ELECTRODE,[45] and ESPResSo[46] provide practical implementations for studying electrochemical interfaces, considering different polarization models.

A confinement by metal electrodes increases the ionic current induced by the external electric field, compared to confinement by the dielectric surfaces.[47–49] This has recently been examined,[49] using the approach originally developed to study the lattice models of ionic liquids.[35] Due to the poor convergence of the effective interaction potential, this approach, however, is only useful for very highly confined ionic liquids, with separation between the electrodes comparable to the ionic diameter. In the present paper, we present a new approach that can be used to simulate ionic fluids confined by polarizable metal surfaces of arbitrary separation. As a proof of concept, we will use the new method to calculate the differential

Published under an exclusive license by AIP Publishing

capacitance (DC) of an ionic liquid confined by polarizable metal electrodes. The new approach uses a combination of Monte Carlo and Molecular Dynamics (MC/MD) simulations to efficiently probe the charge fluctuations on the electrodes, in order to accurately calculate the DC of the system. We will also compare a continuum model of ionic capacitor to a well-studied lattice model,[35] permitting us to explore the limitations of lattice model approximations that are often used to study ionic liquids.[35,38,50–54] The methodological innovation also permits us to easily study the dynamics in systems with varying degrees of confinement, thereby advancing our comprehension of electrochemical processes in charged systems confined by conducting surfaces. This paper is structured as follows: In Sec. II, the model and calculations are presented. Section III is dedicated to the simulation details. The results and conclusions are discussed in Secs. IV and V, respectively.

II. MODEL AND CALCULATIONS

Consider a charge q_i located at $\mathbf{r}_i = (x_i, y_i, z_i)$ in a region between two grounded perfectly conducting planar surfaces located at $-L/2$ and $L/2$. The dielectric constant in between the two electrodes is ε; see Fig. 1. The distances with *tilde* on top are dimensionless, scaled with the separation between the metal plates L, for example, the longitudinal coordinate $\tilde{\rho} = \rho/L$ and the transverse coordinate $\tilde{z} = z/L$. The electrostatic potential generated by the charge is obtained from the solution of Poisson equation,[35,55]

$$\nabla^2 G(\mathbf{r}, \mathbf{r}_i) = -\frac{4\pi q_i}{\varepsilon}\delta(\mathbf{r} - \mathbf{r}_i), \tag{1}$$

where $\mathbf{r} = (x, y, z)$. If the surfaces are grounded, the Dirichlet boundary condition, $G = 0$, needs to be satisfied on each surface. Using the cylindrical coordinate system (see Fig. 1) and the azimuthal symmetry, the three-dimensional delta function can be written as

$$\delta(\mathbf{r} - \mathbf{r}_i) = \frac{1}{2\pi\rho}\delta(\rho)\delta(z - z_i)\,, \tag{2}$$

where the longitudinal distance from the source ion is given by

$$\rho = \sqrt{(x - x_i)^2 + (y - y_i)^2}. \tag{3}$$

It is convenient to expand $\delta(z - z_i)$ in terms of the basis functions that satisfy the Dirichlet boundary condition on the grounded metal surfaces,

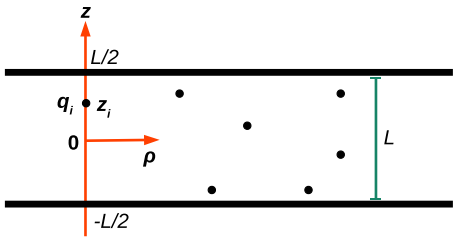


FIG. 1. Charge q_i located between two conducting surfaces separated by distance L.

$$\delta(z - z_i) = \frac{2}{L}\sum_{n=1}^{\infty} \sin\left[n\pi\left(\frac{z}{L} + \frac{1}{2}\right)\right]\sin\left[n\pi\left(\frac{z_i}{L} + \frac{1}{2}\right)\right]. \tag{4}$$

The Green function can then be written as

$$G(\rho, z, z_i) = \frac{2q_i}{\varepsilon L}\sum_{n=1}^{\infty} g_n(\rho)\sin\left[n\pi\left(\frac{z}{L} + \frac{1}{2}\right)\right]\sin\left[n\pi\left(\frac{z_i}{L} + \frac{1}{2}\right)\right]. \tag{5}$$

Substituting this into the Poisson equation, we find that $g_n(\rho)$ satisfies

$$\frac{1}{\rho}\frac{d}{d\rho}\left(\rho\frac{dg_n(\rho)}{d\rho}\right) - k_n^2 g_n(\rho) = -\frac{2}{\rho}\delta(\rho), \tag{6}$$

where $k_n = n\pi/L$. The general solution of Eq. (6) is $g_n(\rho) = C_1 I_0(k_n\rho) + C_2 K_0(k_n\rho)$, where I_0 and K_0 are the modified Bessel functions of first and second kind, respectively. The constant C_1 is 0, since the potential must vanish as $\rho \to \infty$. The singular part of the potential requires $C_2 = 2$. The electrostatic potential produced by the charge—the Green function[35,56–58]—is then

$$G_>(\rho, z, z_i) = \left(\frac{q_i}{\varepsilon L}\right)\sum_{n=1}^{\infty} 4K_0(\pi n\tilde{\rho})\sin\left[\pi n\left(\tilde{z} + \frac{1}{2}\right)\right]\sin\left[\pi n\left(\tilde{z}_i + \frac{1}{2}\right)\right]. \tag{7}$$

As $\tilde{\rho} \to 0$, more and more terms are needed in the summation to achieve a desired accuracy. For large radial separations, however, Eq. (7) can be used efficiently with very small $n_{\max}$—this is the reason we included the subscript $>$ in G. A single term ($n = 1$) is sufficient for separations $\tilde{\rho} > 0.8$. This approximation has recently been employed in the study of ionic conductivity between metal surfaces using the primitive model of electrolyte.[49] In that specific case, the confinement was comparable to the ionic diameter, meaning that the limit $\tilde{\rho} \to 0$ could never be reached. To derive an accurate expression for G for distances $\tilde{\rho} \le 0.8$, we use the integral representation of the delta function,[35,55]

$$\frac{\delta(\rho)}{\rho} = \int_0^{\infty} kJ_0(k\rho)dk, \tag{8}$$

where J_0 is the Bessel function of the first kind. Writing the Green function as

$$G(\rho, z, z_i) = \frac{q_i}{\varepsilon}\int_0^{\infty} kJ_0(k\rho)g_k(z, z_i)dk \tag{9}$$

and substituting into the Poisson equation, we find that $g_k(z, z_i)$ satisfies

$$\frac{d^2 g_k(z, z_i)}{dz^2} - k^2 g_k(z, z_i) = -2\delta(z - z_i). \tag{10}$$

Solving this equation for Dirichlet boundary conditions, we obtain

$$G(\rho, z, z_i) = \left(\frac{q_i}{\varepsilon L}\right)\int_{\tilde{k}=0}^{\infty} d\tilde{k}J_0(\tilde{k}\tilde{\rho})\frac{\cosh\left[\tilde{k}(1 - \tilde{u})\right] - \cosh\left[\tilde{k}\tilde{w}\right]}{\sinh\left(\tilde{k}\right)}, \tag{11}$$

01 December 2025 18:34:50

Published under an exclusive license by AIP Publishing

where $u = |z - z_i|$, $w = z + z_i$, and $\tilde{k} = kL$. To improve the convergence of this integral, we will remove the singular contributions associated with the Coulomb potential produced by the ion itself and by its first images inside the two conducting surfaces,

$$\frac{1}{\sqrt{(\tilde{\rho}^2 + \tilde{u}^2)}} = \int_{\tilde{k}=0}^{\infty} d\tilde{k}\, J_0(\tilde{k}\tilde{\rho}) e^{-\tilde{k}\tilde{u}}, \tag{12}$$

$$-\frac{1}{\sqrt{(\tilde{\rho}^2 + (1-\tilde{w})^2)}} = -\int_{\tilde{k}=0}^{\infty} d\tilde{k}\, J_0(\tilde{k}\tilde{\rho}) e^{-\tilde{k}(1-\tilde{w})}, \tag{13}$$

$$-\frac{1}{\sqrt{(\tilde{\rho}^2 + (1+\tilde{w})^2)}} = -\int_{\tilde{k}=0}^{\infty} d\tilde{k}\, J_0(\tilde{k}\tilde{\rho}) e^{-\tilde{k}(1+\tilde{w})}. \tag{14}$$

Note that images inside the conductor have an opposite sign to the ion. Subtracting the integral representations of these potentials in Eq. (11) and adding their analytical counterpart, we obtain

$$G(\rho, z, z_i) = \left(\frac{q_i}{\varepsilon L}\right)\left[\frac{1}{\sqrt{(\tilde{\rho}^2 + \tilde{u}^2)}} - \frac{1}{\sqrt{(\tilde{\rho}^2 + (1-\tilde{w})^2)}} - \frac{1}{\sqrt{(\tilde{\rho}^2 + (1+\tilde{w})^2)}} + \int_{\tilde{k}=0}^{\infty} d\tilde{k}\, J_0(\tilde{k}\tilde{\rho}) \times \left(\cosh(\tilde{k}\tilde{u})[1 + \coth(\tilde{k})] - \frac{\cosh(\tilde{k}\tilde{w})}{\sinh(\tilde{k})}\right) e^{-2\tilde{k}}\right]. \tag{15}$$

This expression is the exact representation of the Green function that can be used for arbitrary separations between ions. However, it is not very convenient for performing MD or MC simulations, since it requires calculating the integral for each pair interaction. For large separations, however, we already have a very accurate expression for the interaction potential given by Eq. (7). Therefore, we only require an accurate expression for short separations between ions. This can be obtained by expanding the Bessel function inside Eq. (15) until fourth order in ρ and then performing the integral. The integral can be done explicitly in terms of special functions. However, since we only require a short distance behavior, it is sufficient to expand these to fourth order in w and u. The expansion of the Green function, exact to fourth order in ρ, w, and u, is then

$$G_<^{ap}(\rho, z, z_i) = \left(\frac{q_i}{\varepsilon L}\right)\left[(a_0 + b_0\tilde{\rho}^2 + c_0\tilde{\rho}^4) + (a_1 + b_1\tilde{\rho}^2 + c_1\tilde{\rho}^4)(\tilde{z} + \tilde{z}_i)^2 + (a_2 + b_2\tilde{\rho}^2 + c_2\tilde{\rho}^4)(\tilde{z} + \tilde{z}_i)^4 + (a_3 + b_3\tilde{\rho}^2 + c_3\tilde{\rho}^4)(\tilde{z} - \tilde{z}_i)^2 + (a_4 + b_4\tilde{\rho}^2 + c_4\tilde{\rho}^4)(\tilde{z} - \tilde{z}_i)^4 + \frac{1}{\sqrt{(\tilde{\rho}^2 + \tilde{u}^2)}} - \frac{1}{\sqrt{(\tilde{\rho}^2 + (1-\tilde{w})^2)}} - \frac{1}{\sqrt{(\tilde{\rho}^2 + (1+\tilde{w})^2)}}\right]. \tag{16}$$

The coefficients are presented in Table I.

TABLE I. Coefficients of Eq. (16). The constant γ_e is the Euler–Mascheroni constant, $\psi(n, x)$ is the polygamma function, and $\zeta(n)$ is the Riemann zeta function.

$a_0 = \gamma_e + \psi(0, \frac{3}{2})$	$b_0 = \frac{3\zeta(3)}{4} - 1$	$c_0 = \frac{3}{4} - \frac{45\zeta(5)}{64}$
$a_1 = \frac{\psi(2, \frac{3}{2})}{8}$	$b_1 = \frac{93\zeta(5)}{16} - 6$	$c_1 = \frac{45}{4} - \frac{5715\zeta(7)}{512}$
$a_2 = \frac{\psi(4, \frac{3}{2})}{384}$	$b_2 = -15 + \frac{1905\zeta(7)}{128}$	$c_2 = \frac{105}{2} - \frac{53\,655\zeta(9)}{1024}$
$a_3 = \frac{\zeta(3)}{4}$	$b_3 = -\frac{3\zeta(5)}{16}$	$c_3 = \frac{45\zeta(7)}{512}$
$a_4 = \frac{\zeta(5)}{16}$	$b_4 = -\frac{15\zeta(7)}{128}$	$c_4 = \frac{105\zeta(9)}{1024}$

This expression is very accurate as long as $\tilde{\rho} \le 0.8$. The Green function valid for an arbitrary separation between source and field points can then be written as

$$G(\rho, z, z_i) = \begin{cases} G_<^{ap}(\rho, z, z_i) & \text{if } \tilde{\rho} \le 0.8, \\ G_>(\rho, z, z_i) & \text{if } \tilde{\rho} > 0.8. \end{cases}$$

This expression is very efficient for performing computer simulations of Coulomb systems confined by polarizable metal surfaces. Recall that for $\tilde{\rho} > 0.8$, a single term $(n = 1)$ in the sum, Eq. (7), is already sufficient to get very good accuracy, while for short separations, we have a simple algebraic expression for the interaction potential, Eq. (16). Comparing the CPU time for calculating the interaction potential between two ions using the approach presented in this paper with one based on Ewald summation with correction for slab geometry[5] for a non-polarizable system, the present calculation is at least two orders of magnitude faster. In the non-polarizable system, the surface polarization is absent since there is no dielectric mismatch between the confined region and the confining surfaces. We also note that the Green function depends explicitly on the distance of ions from the electrodes as well as on the separation between the ions. Meanwhile, the existing software packages generally assume isotropic interaction potential between the charges. In the future, we intend to implement our method in one of these packages.

An ion of charge q_i placed between two grounded metal surfaces will induce a non-uniformly distributed surface charge. The total induced charge on the left and right surfaces can be calculated explicitly,[35]

$$q_l = -q_i\left(\frac{1}{2} - \tilde{z}_i\right) \text{ and } q_r = -q_i\left(\frac{1}{2} + \tilde{z}_i\right). \tag{17}$$

If instead of being grounded, the surfaces are connected to a battery—so that the electrostatic potential difference between them is *fixed* at ψ_0—the ions will also be influenced by the external electrostatic potential,

$$\phi_s(z) = \psi_0 \tilde{z}, \tag{18}$$

where we have defined the potential to be $\mp\psi_0/2$ on the left and right electrodes, respectively. Using the Gauss law, we can then determine the total charge on the left and right surfaces, respectively, to be

01 December 2025 18:34:50

Published under an exclusive license by AIP Publishing

$$Q_{l,r} = \mp \frac{\varepsilon \psi_0 A}{4\pi L} + q_{l,r}, \tag{19}$$

where A is the electrode area.

III. MODEL AND SIMULATION DETAILS

We model an ionic capacitor using the primitive model of electrolyte. Molecular dynamics simulations of N charged particles are performed inside a box with dimensions $L_{xy} = 140$ Å and $L = 200$ Å. Electrodes are placed at $z = -L/2$ and $z = L/2$, where reflective boundary conditions are applied.[59] The system is periodically replicated in the x and y directions;[35] however, the minimum image convention can be used in most applications. For the parameters $\ell_B/L < 1$—where the Bjerrum length is $\ell_B = e^2/\varepsilon k_B T$, e is the proton charge, k_B is the Boltzmann constant, and T is the temperature—such as the ones studied in the present paper, $\ell_B/L = 0.14$, we only need to use $G_<^{ap}$ due to the short-range nature of the potential. For example, consider two ions at $z = 0$ between surfaces. The potential $G_<^{ap}$ yields ~$0.03k_BT$ for a radial ionic separation of $0.8L$, meaning that we are able to define the radial cutoff at this distance or even smaller. If the parameter l_B/L is not small, such as in vacuum at small surface separations, it is necessary to adjust L_{xy} to apply the minimum image convention correctly, or use more replicas of the main simulation box.[35] The periodic Green function for an infinitely replicated source charge between two grounded conductors can be written as[35]

$$G_p(x, y, z; x_i, y_i, z_i) = \sum_{\mathbf{m}=-\infty}^{\infty} G(\rho_{\mathbf{m}}, z, z_i), \tag{20}$$

where $\rho_{\mathbf{m}} = \sqrt{(x_i - x + m_x L_{xy})^2 + (y_i - y + m_y L_{xy})^2}$ and $\mathbf{m} = (m_x, m_y)$.

The N charged particles consist of N_+ cations of charge q_+ and radius r_+ and N_- anions of charge q_- and radius r_-. The volume fraction occupied by the ions is defined as $\gamma = (N_+V_+ + N_-V_-)/V$, where V_+ and V_- are the effective ionic volumes of the cations and anions, respectively, while V is the volume of the simulation box. The medium is considered to be an organic solvent with uniform dielectric constant $\varepsilon = 20\varepsilon_0$ so that $\ell_B = 28.56$ Å at room temperature. As indicated in previous studies,[60–63] the dielectric constant exhibits an anisotropic behavior near interfaces. To circumvent this issue, the present method can be applied directly in all atom simulations, considering that the atomistic structure of electrodes can be replaced by continuum conducting surfaces, as tested before in other context.[49] Extension of the present method to atomistic simulations will be the subject for the future work. To avoid the overlap between ions, all particles also interact through a truncated Lennard-Jones potential of the Weeks–Chandler–Andersen (WCA) form.[64] For interactions between the same ions, the Lennard-Jones parameter is $\sigma_{LJ} = 2r_+$ for cations and $\sigma_{LJ} = 2r_-$ for anions. For interactions between cations and anions, $\sigma_{LJ} = (r_+ + r_-)$. The strength of this potential is taken to be $\varepsilon_{LJ} = 1k_BT$, and the cutoff radius is $r_{LJ} = 2^{1/6}\sigma_{LJ}$.

In the case of electrodes, the left and right surfaces are antisymmetrically charged, $Q_l = -Q_r$. We set the charge on the right electrode within the simulation box to be $Q_r = Qe$ so that using Eq. (19),

$$Qe = \frac{\varepsilon \psi_0 L_{xy}^2}{4\pi L} - \sum_{i=1}^{N} q_i \tilde{z}_i. \tag{21}$$

The potential difference between the electrodes ψ_0 is then

$$\psi_0 = \frac{4\pi L}{\varepsilon L_{xy}^2}\left[Qe + \sum_{i=1}^{N} q_i \tilde{z}_i\right]. \tag{22}$$

Suppose that the ionic capacitor is charged to carry $-Qe$ and Qe on the left and right surfaces, respectively, and then disconnected from the battery. For a given configuration of ions, the total electrostatic energy will be[35]

$$E(Q) = \frac{1}{2}\sum_{i=1}^{N}\sum_{j=1}^{N} q_j G_p(x_j, y_j, z_j; x_i, y_i, z_i) - \frac{1}{2}\sum_{i=1}^{N}\sum_{j=1}^{N} \frac{q_i q_j \delta_{ij}}{\varepsilon\sqrt{\rho_0^2 + (z_i - z_j)^2}} + \frac{1}{2}\sum_{i=1}^{N} q_i \phi_s(z_i) + \frac{1}{2}\psi_0 Qe. \tag{23}$$

The term with the Kronecker delta is used to subtract the divergent part of ionic self-energy. If the electrodes are disconnected from the battery, as ions move, the total charge on each electrode will remain fixed, while the potential difference between the two electrodes will fluctuate. The electrostatic energy of such an ionic capacitor is[50]

$$E(Q) = \sum_{i=1}^{N}\sum_{j>i}^{N} q_j G_p(x_j, y_j, z_j; x_i, y_i, z_i) + \frac{1}{2}\sum_{i=1}^{N} q_i \phi_{self}(z_i) + \frac{2\pi L}{\varepsilon L_{xy}^2}\left[Qe + \sum_{i=1}^{N} q_i \tilde{z}_i\right]^2, \tag{24}$$

where the interaction potential of the ion with the induced charge on the two electrodes and with its own replicas is

$$\phi_{self}(z_i) = \left(\frac{q_i}{\varepsilon L}\right)\left[a_0 + 4a_1\tilde{z}_i^2 + 16a_2\tilde{z}_i^4 - \frac{1}{\sqrt{(1 - 2\tilde{z}_i)^2}} - \frac{1}{\sqrt{(1 + 2\tilde{z}_i)^2}}\right] + {\sum_{\mathbf{m}}}' G(d_{\mathbf{m}}, z_i, z_i), \tag{25}$$

where the prime excludes the simulation cell $(m_x = 0, m_y = 0)$ from summation and $d_{\mathbf{m}} = \sqrt{m_x^2 L_{xy}^2 + m_y^2 L_{xy}}$. As already mentioned, in many applications, the periodic Green function in Eq. (24) can be approximated by $G_p(x_j, y_j, z_j;\ x_i, y_i, z_i) \approx G(\rho, z_i, z_j)$, with the summation over replicas substituted by the minimum image convention.

The simulations are carried out using a mixed method: Langevin thermostat molecular dynamics simulation (MD) for ionic motion and the constant potential ensemble Monte Carlo simulation (MC) to account for the electrode charge fluctuations. The constant potential ensemble is chosen because the fluctuation of the electrode

01 December 2025 18:34:50

Published under an exclusive license by AIP Publishing

charge can be directly related to the DC, providing us with an easy access to this important quantity. We could also work in the constant charge ensemble; however, the statistical error intrinsic to the calculation of the electrostatic potential difference in this ensemble makes the calculation of DC less accurate.

The integration of Langevin equation of motion is performed using the velocity-Verlet algorithm, with a time step $dt = 0.001(m\beta)^{1/2}L$, where m is the ion mass. If the electrodes are connected to a battery with a potential difference ψ, the thermodynamics of the system is determined by the configurational partition function in the constant ψ ensemble,

$$Z[T,\psi] = \int \Pi_{i=1}^{N} d\mathbf{r}_i \int e^{-\beta E(Q)+\beta Qe\psi} dQ. \tag{26}$$

Note that in order to calculate the partition function of a system kept at a fixed potential ψ, we require electrostatic energy $E(Q)$ for electrodes of *total charge* Q—i.e., Eq. (23). Also note that the distribution of charge over the electrode surfaces changes with ionic motion.[65] Using the usual detailed balance argument, a change in the electrode charge $\Delta Q = (1 - 2R_N)$, where R_N is a uniform random number from 0 to 1, is attempted every 500 MD steps. The acceptance probability for MC move follows from Eq. (26) and can be expressed as

$$P = \min\left[1, e^{-\beta[E(Q+\Delta Q)-E(Q)]+\beta\Delta Qe\psi}\right]. \tag{27}$$

Using Eq. (27), the differential capacitance (DC) can be shown to be related to the fluctuation of the electrode charge, while the potential difference ψ between the electrodes is kept fixed by an external battery,

$$C = \frac{1}{L_{xy}^2}\frac{\partial\langle Qe\rangle}{\partial\psi} = \frac{\beta}{L_{xy}^2}\left(\langle(Qe)^2\rangle - \langle Qe\rangle^2\right). \tag{28}$$

We stress that the choice of the ensemble in which the potential difference between electrodes is fixed, rather than the charge on each electrode, is primarily due to the accuracy of the calculation of DC. In the thermodynamic limit, both ensembles are equivalent—in practice, however, the accuracy of results calculated using the constant potential difference ensemble is superior. We also note that in the experiments, one usually controls the potential difference between the electrodes and not their charge.[66] The equilibrium takes $\sim 5 \times 10^5$ MD time steps to reach. The criterion for equilibrium is the electrode charge stability. The statistical analysis is performed over the 5×10^4 samples, obtained at intervals of 5×10^2 MD time steps, in order to discorrelate the sample.

IV. RESULTS

As a first example, we study a symmetric 1:1 electrolyte with ionic radii, $r_+ = r_- = 5$ Å. The ionic density profiles are shown in Fig. 2(a). Some structuring in the double layers near the surfaces can be observed. Besides the surface potential, the surface polarization contributes to ionic adsorption to the electrodes.[67–73] This can be observed in Fig. 3, where the concentration profiles for non-polarizable and polarizable surfaces are compared. The average charge Q and DC are shown in Fig. 4 (purple circles). The maximum DC occurs at zero voltage, decreasing as the absolute voltage increases. Next, we consider a 1:1 electrolyte of different ionic sizes, $r_+ = 3$ Å and $r_- = 5$ Å, for the same parameters as in the previous case. The ionic density profiles are shown in Fig. 2(b). The DC is enhanced when compared to the case of symmetric electrolyte; see Fig. 4 (maroon diamonds). A more significant increase in DC is observed for the charge asymmetric 3:1 electrolyte; see green square data in Fig. 4. The ionic density profiles are very asymmetric, with strong layering effects at the cathode; see Fig. 2(c).

For the monovalent symmetric electrolyte at high concentrations, DC has a characteristic bell-shape. As the concentration is lowered, we observe a crossover to a camel-shaped DC. Close to $\gamma = 1/20$, the camel-shaped DC profile begins to appear, and at lower γ's, we see a clear local minimum in DC at $\psi = 0$; see Fig. 5(a). We also observe that at high voltages, DC is very low for dilute electrolyte, while it remains very significant for concentrated electrolyte solutions; see Fig. 5(b). This sharp transition is related to the ability of electrolyte to screen the electric field produced by the electrodes. At low γ, there are not enough ions inside the system to compensate the charge on the electrodes. Therefore, the potential

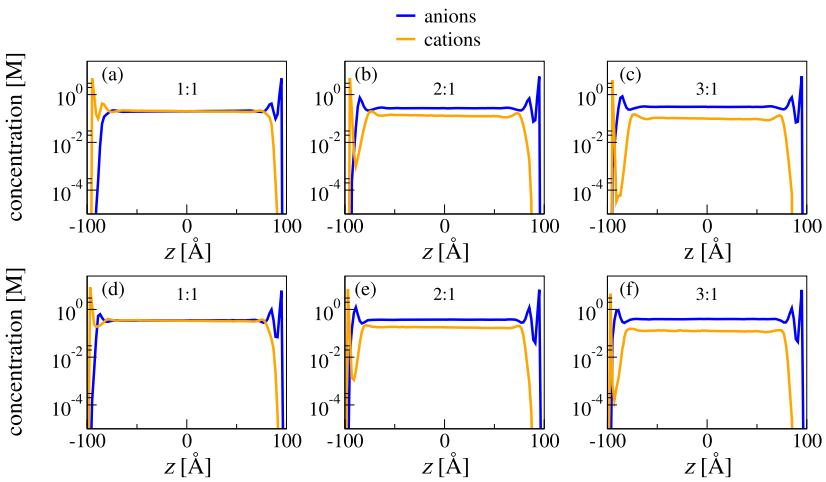


FIG. 2. Ionic concentration profiles for different electrolyte configurations at $\gamma = 3/20$. The top panels represent the symmetric electrolytes with radii $r_+ = r_- = 5$ Å: (a) 1:1, (b) 2:1, and (c) 3:1 electrolytes. The bottom panels represent the asymmetric electrolytes with radii $r_+ = 3$ Å and $r_- = 5$ Å: (d) 1:1, (e) 2:1, and (f) 3:1 electrolytes. The electrostatic potential difference between the electrodes is $\psi = 1$ V for all cases.

01 December 2025 18:34:50

Published under an exclusive license by AIP Publishing

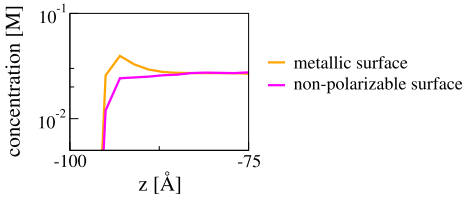


FIG. 3. Concentration profiles for a 1:1 symmetric electrolyte with ion radii of $r_+ = r_- = 5$ Å on non-polarizable and metallic surfaces, at $\gamma = 1/60$. There is no electrostatic potential difference between the electrodes, i.e., $\psi = 0$ V. Only the cation concentrations are shown.

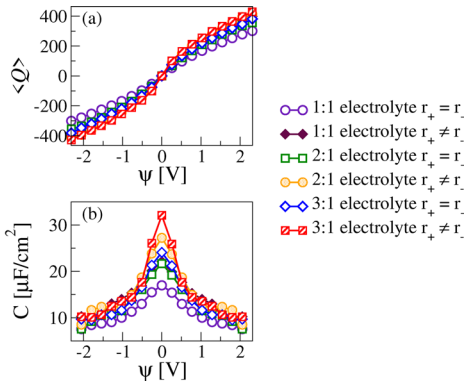


FIG. 4. (a) Average surface charge Qe and (b) differential capacitance (DC) for the same parameters as in Fig. 2.

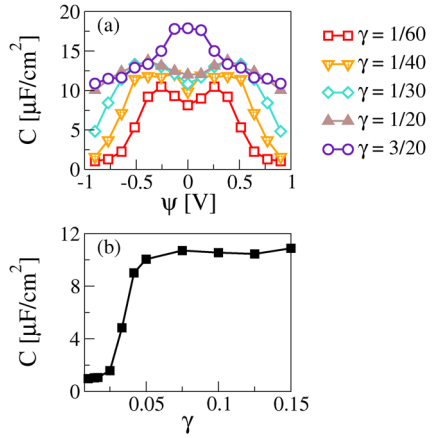


FIG. 5. (a) DC for a lot of values of γ for a symmetric 1:1 electrolyte with ionic radius $r_+ = r_- = 5$ Å. (b) DC as a function of γ for $\psi = 0.9$ V, where a sharp transition between low and high DC can be observed.

drop occurs over the distance of separation between the electrodes. Meanwhile, when the total cation (anion) charge inside the system equals or is greater than the charge on cathode (anode), there is a qualitative change in the behavior of DC. The potential drop in such systems will be restricted to the distance comparable to the Debye length from the electrodes. In the strong coupling limit, the drop will happen over the length of Stern layer around each electrode. We can roughly approximate this width by the ionic radius. The total capacitance will then be equal to that of two planar capacitors connected in series. Performing the calculation, we find that the capacitance of this limiting case is 18 μF/cm^2, while in simulations, we observe the saturated value to be 11 μF/cm^2; see Fig. 5. The difference between the two values can be attributed to the fact that hardcore repulsion between the ions, as well as thermal fluctuations, will in general prevent the Stern layer from neutralizing the charge on the electrodes. If we suppose that neutralization of the electrode charge happens over the distance of $d \approx 1.5r_i$, where r_i is the ionic radius, then we will obtain the capacitance value very close to the one observed in simulations. The transition between low and high DC—at large voltages—agrees precisely with the value of γ at which the number of ions inside the system becomes sufficient to neutralize the electrode charge.

It is also interesting to compare the present continuum model with the lattice model of ionic capacitor developed in Ref. 35 for 1:1 electrolyte with ions of the same sizes, but restricted to move on a cubic grid. In this model, the simulation space is organized into a lattice, with each node designated as a possible ion position. These positions are arranged at intervals corresponding to the typical diameters of ions. The electrostatic interactions between ions are calculated using either periodic Green functions[35] or the present method. During the MC simulation, ions can move to an empty node or interchange positions. More details can be obtained in the original work.[35] We see that lattice and continuum models show significant differences in both Q and DC vs ψ curves. In particular, the lattice model significantly overestimates the maximum value of DC at zero voltage for highly concentrated systems; see Figs. 6(a)

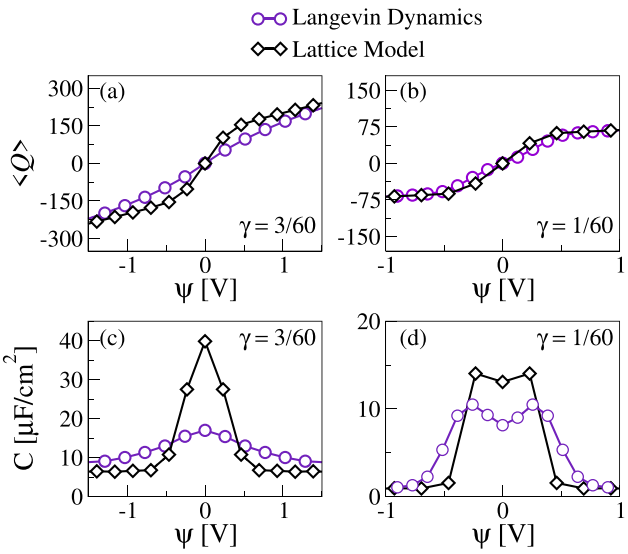


FIG. 6. Average surface charge Qe and DC of a symmetric 1:1 electrolyte with ionic radii $r_+ = r_- = 5$ Å for continuum and lattice models. (a) Qe for $\gamma = 3/60$, (b) Qe for $\gamma = 1/60$, (c) DC for $\gamma = 3/60$, and (d) DC for $\gamma = 1/60$. The indigo circles represent the Langevin dynamics results, while the black diamonds represent the lattice model data.

01 December 2025 18:34:50

Published under an exclusive license by AIP Publishing

and 6(c). For low volume fractions of electrolyte, the agreement improves; see Figs. 6(b) and 6(d). At infinite dilution, we expect to see a full agreement. However, for parameters relevant to ionic supercapacitors, we see that there is a very significant difference between lattice and continuum models. These findings are also consistent with the analytical comparisons performed on 2D systems in Ref. 74.

V. CONCLUSIONS

We have presented a method to efficiently simulate electrolyte solutions confined between polarizable electrodes. Our approach is particularly useful for studying ionic liquids for which a fourth order expansion of the interaction potential provides a very accurate approximation to the full Green function. We have applied the new method to explore the differential capacitance of ionic capacitors, revealing that size and charge asymmetries between cations and anions significantly enhance DC for low voltages. We have also observed the characteristic transition between bell-shaped and camel-shaped DC[75,76] as the volume fraction occupied by the electrolyte is lowered. The new MD/MC simulation method allows us to easily study both dilute and concentrated ionic solutions, permeating efficient calculation of DC. In the present calculation, we have used ideal (perfectly polarizable) metal electrodes. In the future, we intend to explore the effects of non-ideality, which can be incorporated into our calculation of the Green function by replacing the ideal metal by a Thomas–Fermi conductor. However, even without performing any additional calculations, we can approximately include the effects of non-ideality by simply shifting the plane of polarization—at which the Dirichlet boundary conditions are imposed—into the interior of the metal by the amount equal to the Thomas–Fermi screening length. The simple form of the interaction potential between the charges confined by the metal electrodes derived in this paper should also allow us to efficiently study fully atomistic models of ionic capacitors.

ACKNOWLEDGMENTS

This work was partially supported by CNPq and INCT-FCx.

AUTHOR DECLARATIONS

Conflict of Interest

The authors have no conflicts to disclose.

Author Contributions

Igor M. Telles: Data curation (equal); Investigation (equal); Software (equal); Validation (equal); Visualization (equal); Writing – review & editing (equal). **Alexandre P. dos Santos**: Conceptualization (equal); Funding acquisition (equal); Investigation (equal); Methodology (equal); Project administration (equal); Resources (equal); Software (equal); Supervision (equal); Validation (equal); Writing – original draft (equal); Writing – review & editing (equal). **Yan Levin**: Conceptualization (equal); Formal analysis (equal); Funding acquisition (equal); Investigation (equal); Methodology (equal); Project administration (equal); Supervision (equal); Visualization (equal); Writing – original draft (equal); Writing – review & editing (equal).

DATA AVAILABILITY

The data that support the findings of this study are available from the corresponding author upon reasonable request.

REFERENCES

[1] P. P. Ewald, Ann. Phys. **369**, 253 (1921).
[2] I.-C. Yeh and M. L. Berkowitz, J. Chem. Phys. **111**, 3155 (1999).
[3] A. Arnold, J. de Joannis, and C. Holm, J. Chem. Phys. **117**, 2496 (2002).
[4] A. Bródka, Chem. Phys. Lett. **400**, 62 (2004).
[5] A. P. dos Santos, M. Girotto, and Y. Levin, J. Chem. Phys. **144**, 144103 (2016).
[6] A. Arnold and C. Holm, J. Chem. Phys. **123**, 144103 (2005).
[7] I. M. Telles, R. K. Bombardelli, A. P. dos Santos, and Y. Levin, J. Mol. Liq. **336**, 116263 (2021).
[8] I. M. Telles, Y. Levin, and A. P. dos Santos, Langmuir **38**, 3817 (2022).
[9] S. Tyagi, M. Süzen, M. Sega, M. Barbosa, S. S. Kantorovich, and C. Holm, J. Chem. Phys. **132**, 154112 (2010).
[10] V. Jadhao, F. J. Solis, and M. O. de la Cruz, Phys. Rev. Lett. **109**, 223905 (2012).
[11] D. T. Limmer, C. Merlet, M. Salanne, D. Chandler, P. A. Madden, R. van Roij, and B. Rotenberg, Phys. Rev. Lett. **111**, 106102 (2013).
[12] A. Arnold, K. Breitsprecher, F. Fahrenberger, S. Kesselheim, O. Lenz, and C. Holm, Entropy **15**, 4569 (2013).
[13] Y. Jing, V. Jadhao, J. W. Zwanikken, and M. Olvera de la Cruz, J. Chem. Phys. **143**, 194508 (2015).
[14] M. Girotto, A. P. dos Santos, and Y. Levin, J. Chem. Phys. **147**, 184105 (2017).
[15] I. M. Telles and A. P. dos Santos, Langmuir **37**, 2104 (2021).
[16] R. K. Bombardelli, I. M. Telles, A. P. dos Santos, and Y. Levin, J. Phys. Chem. B **125**, 11091 (2021).
[17] J. Yuan, H. S. Antila, and E. Luijten, Macromolecules **53**, 2983 (2020).
[18] I. M. Telles, M. Arfan, and A. P. dos Santos, J. Chem. Phys. **158**, 144902 (2023).
[19] A. Bakhshandeh, A. P. dos Santos, and Y. Levin, Phys. Rev. Lett. **107**, 107801 (2011).
[20] A. P. dos Santos and Y. Levin, Phys. Rev. Lett. **122**, 248005 (2019).
[21] M. Arfan, I. M. Telles, and A. P. dos Santos, J. Mol. Liq. **401**, 124527 (2024).
[22] R. M. Lynden-Bell, M. G. Del Pópolo, T. G. A. Youngs, J. Kohanoff, C. G. Hanke, J. B. Harper, and C. C. Pinilla, Acc. Chem. Res. **40**, 1138 (2007).
[23] M. V. Fedorov and A. A. Kornyshev, Chem. Rev. **114**, 2978 (2014).
[24] S. Kondrat, G. Feng, F. Bresme, M. Urbakh, and A. A. Kornyshev, Chem. Rev. **123**, 6668 (2023).
[25] A. Schlaich, D. Jin, B. L, and B. Coasne, Nat. Mater. **21**, 237 (2022).
[26] A. C. Forse, C. Merlet, J. M. Griffin, and C. P. Grey, J. Am. Chem. Soc. **138**, 5731 (2016).
[27] G. S. dos Reis, S. H. Larsson, H. P. de Oliveira, M. Thyrel, and E. C. Lima, Nanomaterials **10**, 1398 (2020).
[28] A. Eftekhari, Energy Storage Mater. **9**, 47 (2017).
[29] M. Salanne, "Ionic liquids for supercapacitor applications," in *Ionic Liquids II* (Springer International Publishing, 2018), pp. 29–53.
[30] L. Scalfi, M. Salanne, and B. Rotenberg, Annu. Rev. Phys. Chem. **72**, 189 (2021).
[31] J. I. Siepmann and M. Sprik, J. Chem. Phys. **102**, 511 (1995).
[32] S. K. Reed, O. J. Lanning, and P. A. Madden, J. Chem. Phys. **126**, 084704 (2007).
[33] C. Merlet, D. T. Limmer, M. Salanne, R. van Roij, P. A. Madden, D. Chandler, and B. Rotenberg, J. Phys. Chem. C **118**, 18291 (2014).
[34] G. Pireddu, L. Scalfi, and B. Rotenberg, J. Chem. Phys. **155**, 204705 (2021).
[35] M. Girotto, A. P. dos Santos, and Y. Levin, J. Chem. Phys. **147**, 074109 (2017).

01 December 2025 18:34:50

Published under an exclusive license by AIP Publishing

[36]S. Stenberg, B. Stenqvist, C. Woodward, and J. Forsman, Phys. Chem. Chem. Phys. **22**, 13659 (2020).
[37]M. Dudka, S. Kondrat, A. Kornyshev, and G. Oshanin, J. Phys.: Condens. Matter **28**, 464007 (2016).
[38]M. Girotto, T. Colla, A. P. dos Santos, and Y. Levin, J. Phys. Chem. B **121**, 6408 (2017).
[39]Y. Groda, M. Dudka, A. A. Kornyshev, G. Oshanin, and S. Kondrat, J. Phys. Chem. C **125**, 4968 (2021).
[40]S. Nair, G. Pireddu, and B. Rotenberg, "Induced charges in a Thomas–Fermi metal: Insights from molecular simulations," Mol. Phys. e2365990 (2024) (published online).
[41]R. S. Sitlapersad, A. R. Thornton, and W. K. den Otter, J. Chem. Phys. **160**, 034107 (2024).
[42]R. S. Sitlapersad, A. R. Thornton, and W. K. den Otter, J. Chem. Phys. **160**, 044111 (2024).
[43]I. L. Geada, H. Ramezani-Dakhel, T. Jamil, M. Sulpizi, and H. Heinz, Nat. Commun. **9**, 716 (2018).
[44]A. Marin-Laflèche, M. Haefele, L. Scalfi, A. Coretti, T. Dufils, G. Jeanmairet, S. Reed, A. Serva, R. Berthin, C. Bacon, S. Bonella, B. Rotenberg, P. Madden, and M. Salanne, J. Open Source Softw. **5**, 2373 (2020).
[45]L. J. V. Ahrens-Iwers, M. Janssen, S. R. Tee, and R. H. Meißner, J. Chem. Phys. **157**, 084801 (2022).
[46]F. Weik, R. Weeber, K. Szuttor, K. Breitsprecher, J. de Graaf, M. Kuron, J. Landsgesell, H. Menke, D. Sean, and C. Holm, Eur. Phys. J.: Spec. Top. **227**, 1789 (2019).
[47]N. Kavokine, P. Robin, and L. Bocquet, J. Chem. Phys. **157**, 114703 (2022).
[48]F. Jiménez-Ángeles, A. Ehlen, and M. Olvera de la Cruz, Faraday Discuss. **246**, 576 (2023).
[49]A. P. dos Santos, F. Jiménez-Ángeles, A. Ehlen, and M. Olvera de la Cruz, Phys. Rev. Res. **5**, 043174 (2023).
[50]M. Girotto, R. M. Malossi, A. P. dos Santos, and Y. Levin, J. Chem. Phys. **148**, 193829 (2018).
[51]A. A. Kornyshev, Faraday Discuss. **164**, 117 (2013).
[52]A. A. Lee, S. Kondrat, and A. A. Kornyshev, Phys. Rev. Lett. **113**, 048701 (2014).
[53]V. Démery, D. S. Dean, T. C. Hammant, R. R. Horgan, and R. Podgornik, J. Chem. Phys. **137**, 064901 (2012).
[54]V. Démery, D. S. Dean, T. C. Hammant, R. R. Horgan, and R. Podgornik, Europhys. Lett. **97**, 28004 (2012).
[55]Y. Levin, Europhys. Lett. **76**, 163 (2006).
[56]J. D. Jackson, *Classical Electrodynamics*, 2nd ed. (Wiley, New York, 1975).
[57]S. Kondrat, N. Georgi, M. V. Fedorov, and A. A. Kornyshev, Phys. Chem. Chem. Phys. **13**, 11359 (2011).
[58]B. Skinner, T. Chen, M. S. Loth, and B. I. Shklovskii, Phys. Rev. E **83**, 056102 (2011).
[59]I. V. Pivkin and G. E. Karniadakis, J. Comput. Phys. **207**, 114 (2005).
[60]D. J. Bonthuis, S. Gekle, and R. R. Netz, Phys. Rev. Lett. **107**, 166102 (2011).
[61]A. Schlaich, E. W. Knapp, and R. R. Netz, Phys. Rev. Lett. **117**, 048001 (2016).
[62]L. Fumagalli, A. Esfandiar, R. Fabregas, S. Hu, P. Ares, A. Janardanan, Q. Yang, B. Radha, T. Taniguchi, K. Watanabe, G. Gomila, K. S. Novoselov, and A. K. Geim, Science **360**, 1339 (2018).
[63]M. H. Motevaselian and N. R. Aluru, J. Phys. Chem. Lett. **11**, 10532 (2020).
[64]J. D. Weeks, D. Chandler, and H. C. Andersen, J. Chem. Phys. **54**, 5237 (1971).
[65]S. R. Tee and D. J. Searles, J. Chem. Theory Comput. **19**, 2758 (2023).
[66]N. G. Hörmann, S. D. Beinlich, and K. Reuter, J. Phys. Chem. C **128**, 5524 (2024).
[67]C. Merlet, C. Péan, B. Rotenberg, P. A. Madden, P. Simon, and M. Salanne, J. Phys. Chem. Lett. **4**, 264 (2013).
[68]K. Breitsprecher, K. Szuttor, and C. Holm, J. Phys. Chem. C **119**, 22445 (2015).
[69]J. B. Haskins and J. W. Lawson, J. Chem. Phys. **144**, 184707 (2016).
[70]J. Gäding, G. Tocci, M. Busch, P. Huber, and R. H. Meißner, J. Chem. Phys. **156**, 064703 (2022).
[71]S. Ntim and M. Sulpizi, Phys. Chem. Chem. Phys. **25**, 22619 (2023).
[72]S. Ntim and M. Sulpizi, J. Phys. Chem. B **128**, 1936 (2024).
[73]A. Reinauer, S. Kondrat, and C. Holm, J. Chem. Phys. **161**, 104101 (2024).
[74]T. Verkholyak, A. Kuzmak, and S. Kondrat, J. Chem. Phys. **155**, 174112 (2021).
[75]M. T. Alam, M. Mominul Islam, T. Okajima, and T. Ohsaka, Electrochem. Commun. **9**, 2370 (2007).
[76]M. Fedorov, N. Georgi, and A. Kornyshev, Electrochem. Commun. **12**, 296 (2010).

01 December 2025 18:34:50

Published under an exclusive license by AIP Publishing